Supporting Information

Moderate Binding between Two SARS-CoV-2 Protein Segments and α-Synuclein Alters Its Toxic Oligomerization Propensity Differently

Vince St. Dollente Mesias,[1] Hongni Zhu,[1] Xiao Tang,[2] Xin Dai,[1] Wei Liu,[3] Yusong Guo,[2] and Jinqing Huang [1,*]

[1]Department of Chemistry, The Hong Kong University of Science and Technology, Clear Water Bay, Hong Kong, China

[2]Division of Life Science, The Hong Kong University of Science and Technology, Clear Water Bay, Hong Kong, China

[3]Department of Chemistry, The University of Hong Kong, Pokfulam Road, Hong Kong, China

[*]Corresponding Author (jqhuang@ust.hk)

Experimental procedures

Preparation of alpha-synuclein

The procedure for the preparation of wild type alpha-synuclein was adopted from our previous work.[1] The recombinant human wild type alpha-synuclein was overexpressed by *E. coli* BL21(DE3) with plasmid pET28a. Cells were grown in Luria broth (LB) medium in the presence of 50 μg/mL Kanamycin and protein expression was induced by 0.3 mM isopropyl β-D-1-thiogalactopyranoside (IPTG). The cell pellet was resuspended in Tris buffer (25 mM Tris-HCl, pH 7.4) and lysed by sonication. After centrifugation at 30000 x g for 45 min at 4 ℃, the supernatant was boiled for to remove most *E. coli* proteins. After centrifugation at 30000 x g for another 60 min at 4 ℃, the supernatant was loaded onto HiPrep DEAE FF 16/10 column (GE Healthcare Biosciences, New Jersey, USA). A gradual sodium chloride gradient was chosen and applied to elute the target protein. After SDS-PAGE gel analysis, fractions containing the target protein were desalted by HiPrep™ 26/10 Desalting column. The desalted solution was loaded onto HiPrep 16/60 Sephacryl S-100 column (GE Healthcare Biosciences, New Jersey, USA) for further purification, with 25 mM Tris-HCl, pH 7.4 as the running buffer. Fractions were analyzed by SDS-PAGE gel, and targeted protein were collected, concentrated and stored at -20 ℃. The concentration of alpha-synuclein was determined by UV-1800 spectrophotometer (SHIMADZU, Kyoto, Japan) with the extinction coefficient of 5960 $cm^{-1}M^{-1}$ at 276 nm.

Preparation of SARS-CoV-2 RBD

The glutathione transferase tagged (GST) SARS-CoV-2-Spike (RBD) purification was performed as described previously.[2] The SARS-CoV-2-RBD was cloned in a pGEX-2T vector (GE Healthcare Biosciences, New Jersey, USA). The constructs were transformed in BL21 cells and individual colonies were grown to O.D. 0.6 in 500 ml of LB medium at 37 °C. Protein expression was induced with 0.5 mM IPTG for 16 h at 25 °C. Cells were centrifuged, washed with PBS and lysed in lysis buffer (50 mM Tris, pH 8.0, 5 mM EDTA, 150 mM NaCl, 10% glycerol, 5 mM dithiothreitol, 0.5 mg/mL lysosome, proteinase inhibitor cocktail, complete, EDTA free, one tablet for 50 ml solution, Roche, Mannheim, Germany). After 30 min on ice, the cell lysates were adjusted to contain 0.5% Triton X-100 and sonicated four times for 30 s each time and centrifuged at 55000 rpm for 20 min in a Beckman TLA-110 rotor for the ultracentrifuge. The supernatant fraction was incubated with 200 μL glutathione-agarose beads at 4°C overnight. After incubation, the beads were washed four times with PBS containing 1 mM DTT and 0.1% Tween 20 then two times with PBS. The bound GST tagged proteins were then eluted using elution buffer (50 mM Tris, pH 8.0, 250 mM KCl, 1 mM DTT, 25 mM glutathione, pH 8.0, proteinase inhibitor cocktail).

Preparation of unilamellar vesicles

The vesicles are widely used because they mimic biological membranes,[3] and its components were purchased from Avanti Polar Lipids Inc. The vesicle is composed of 45% egg phosphatidylcholine, 35% egg phosphatidylethanolamine, 15% heart cardiolipin, and 5% 16:0-18:1 phosphatidylserine, they were dissolved in chloroform. The lipid mixture was doped with Oregon Green-488 DHPE (Invitrogen) at 1000:1 lipid-to-dye ratio, and mixture was purged with nitrogen gas until the chloroform has been evaporated indicated by the presence of the lipid film. The trace amount of chloroform was removed through vacuum oven (Shellab 1445-2, Sheldon Laboratory Systems, Oregon, USA) drying for 4 h at 25 °C. The resulting lipid film was then subjected to the transition temperature based on the lipid components and hydrated by PBS (10 mM sodium phosphate buffer, 138 mM NaCl, 27 mM KCl, pH 7.4) with constant stirring for 1 h at 200 rpm. The hydrated lipid was extruded 21 times using the Avanti Mini

Extruder (Avanti Polar Lipids Inc., Alabama, USA) with 0.1 μm polycarbonate membrane. The resulting small unilamellar vesicles (SUV) was subjected to dynamic light scattering using the ZetaPlus analyzer (Brookhaven Instruments, New York, USA) to obtain the size distribution and polydispersity index (Figure S5).

Isothermal titration calorimetry (ITC)

We utilized a commercial isothermal titration calorimeter (MicroCal PEAQ-ITC, Malvern Panalytical, Malvern, UK) to perform titration experiments. In these experiments, all proteins (αSyn and RBD) were buffer exchanged to PBS using micro bio-spin 6 columns (Bio Rad, California, USA) to prevent the interfering heat signals coming from buffer mismatch. The SK9 peptide, SFYVYSRVK, (98.21% purity; GL Biochem Ltd., Shanghai, China) was prepared by dissolving an appropriate amount in PBS. For the titration of αSyn and RBD, a 95 μM αSyn solution was loaded into the syringe of the ITC instrument and a 9.5 μM solution of RBD was loaded in the calorimetric cell. For the titration of αSyn and SK9, a 200 μM αSyn solution was loaded into the syringe while 20 μM solution of SK9 was loaded in the calorimetric cell. During each ITC experiment, the solutions were equilibrated at 25 °C and 19 injections into the calorimetric cell were carried out while the duration of each injection was 8 s with the interval of 150 s. The volume of each injection was 4 μL and the stirring speed was maintained at 750 rpm. Control experiments such as αSyn to buffer and buffer to proteins (RBD or SK9) titrations were also done to account for non-specific interactions and heat of dilution (Figure S1). The data were analyzed by the MicroCal PEAQ-ITC analysis software.

Circular dichroism (CD) spectroscopy

There are three αSyn systems used in this approach with the following final concentrations: (1) αSyn-RBD (5 μM αSyn and 0.1 μM RBD, in PBS); (2) αSyn-SK9 (5 μM αSyn and 5 μM SK9, in PBS); and αSyn control (5 μM in PBS). These systems were incubated in an orbital shaker at 200 rpm for 6 d at 30 °C, the CD spectral analysis were performed for each system on a daily basis. The CD spectra were obtained using the Chirascan Spectrometer (Applied Photophysics, Leatherhead, UK) with solvent background correction from 200 nm to 800 nm and smoothed by Savitzky-Golay filter. Each spectrum is an average of 10 scans. The secondary structure analysis was performed using the BeStSel algorithm[4,5] for day 0, day 3, and day 6 CD spectra of all systems (Figure S2 and Table S1). Control experiments with either RBD or SK9 alone at the same concentration in their respective mixtures were also conducted (Figure S3).

Thioflavin T (ThT) aggregation assay

The αSyn systems identical to the CD experiment were added with 5 μM ThT and incubated in an orbital shaker at 200 rpm for 6 d at 30 °C. An additional αSyn sample of similar concentration was added with 10 mM Mg^{2+} ions to deliberately cause fibrillation was also analyzed. To follow the formation of αSyn fibrils, the increase in fluorescence was measured by FlexStation 3 Multi-mode Microplate reader (Molecular Devices LLC, California, USA) for every 3 h for the first 24 h and for every 6 h for the rest of incubation period (Figure S4). The ThT was excited at 446 nm and the signal was measured at 485 nm.

Fluorescence leakage assay

The leakage of SUV was measured in FlexStation 3 Multi-mode Microplate reader (Molecular Devices LLC, California, USA), with an excitation wavelength at 501 nm and emission at 526 nm. Three αSyn systems with similar concentrations were incubated according to the CD experiment, and added to the SUV solution. Samples were kept at a constant 25 °C. Before measurements, each SUV solution contained 10 mM DPX quencher (Invitrogen, Thermo Fischer Scientific Corp., USA) with a reduced salt concentration to keep solution equiosmotic.

The fluorescence measurements were conducted for 12000 s with the interval of 150 s. Control experiments were performed to obtain the leakage profile of the SUV alone, and the addition of 0.1% Triton X-100 was done for the leakage profile of the fully disrupted SUV (Figure S6) The unleaked fraction was calculated using the formula below (eq S1). The leakage profiles were plotted as the fraction unleaked against time, and were fitted with single exponential decay through the Levenberg-Marquardt algorithm to obtain the rate constants (Figures S7-S9 and Table S2).

Equation S1.

$$\text{fraction unleaked} = 1 - \frac{F_0 - F}{F_{max}}$$

F_0- F: the difference between the SUV control signal and the sample signal at time t,
F_{max}: the SUV signal upon the addition of Triton X-100

The leakage profiles are generated in triplicates. The Whisker plot of the rate constants and the subsequent paired comparison plot (two-way ANOVA, p-value with bracket) were obtained using OriginPro 2022.

Protein-protein/peptide docking

To search for the suitable models, we adopted the equilibrated monomeric αSyn configurations generated from the previous simulations, 3000 ns molecular dynamics simulation at 310 K by Hansmann and co-workers, which are all published as supplemental material of a recent paper on αSyn-SK9 interactions,[6] and docked them to RBD and SK9. The wildtype RBD model was retrieved from the Chain B of PDB: 7C8D and the Omicron (BA.5) RBD was retrieved from the Chain E of PDB: 7ZXU. The SK9 model was obtained using *de novo* peptide modelling. The molecular docking for αSyn-RBD and αSyn-SK9 systems were done using the High-ambiguity driven protein-protein docking 2.4 (HADDOCK 2.4) followed by model refinement.[7,8] The models were subjected to binding energy and binding affinity analysis via Protein binding energy prediction (PRODIGY),[9,10] and the accepted models were determined by matching with the experimental data. The binding interface of each model was analyzed through the Protein database summaries (PDBsum).[11]

The model was validated by changing the residues around the interface through mutation followed by another experimental binding measurement. The wildtype RBD was replaced by the RBD of the latest Omicron subvariant BA.5 (Sino Biological, Shanghai, China) which contains 17 mutations within the RBD and subjected to isothermal titration calorimetry with alpha synuclein in similar conditions as described in the text.

Supporting Figures and Tables

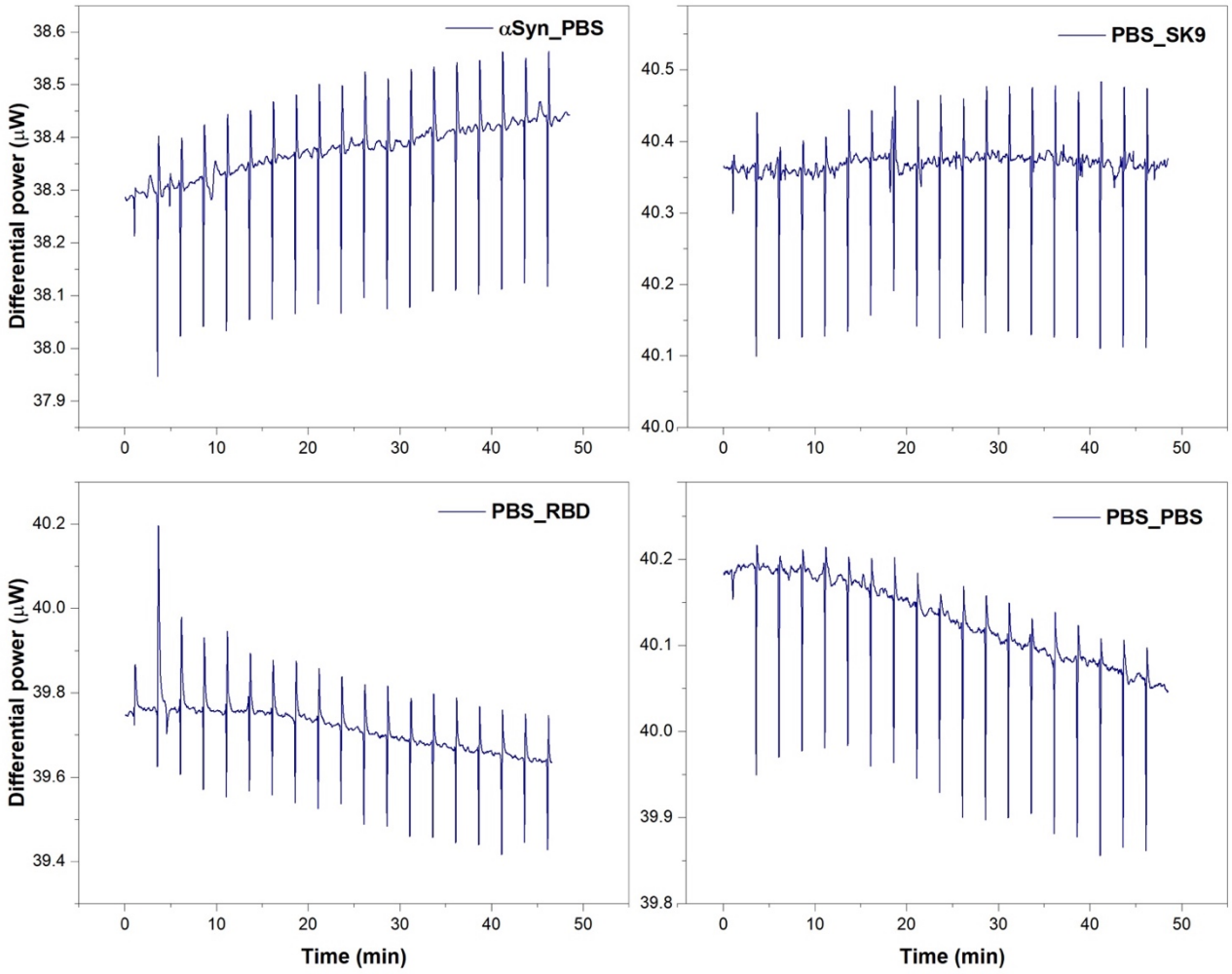

Figure S1. Isothermal titration calorimetry control runs. Each run has similar conditions with the protein-protein titration (injections = 19, equilibrium temperature = 25 °C, injection volume = 4 μL, injection time = 8 s, injection interval = 150 s, and stirring rate = 750 rpm). A.) Titration of PBS in the calorimetric cell by the αSyn solution in the syringe. B.) Titration of SK9 solution in the calorimetric cell by the PBS in the syringe. C.) Titration of RBD solution in the calorimetric cell by the PBS in the syringe. D.) Titration of PBS in the calorimetric cell by the PBS in the syringe.

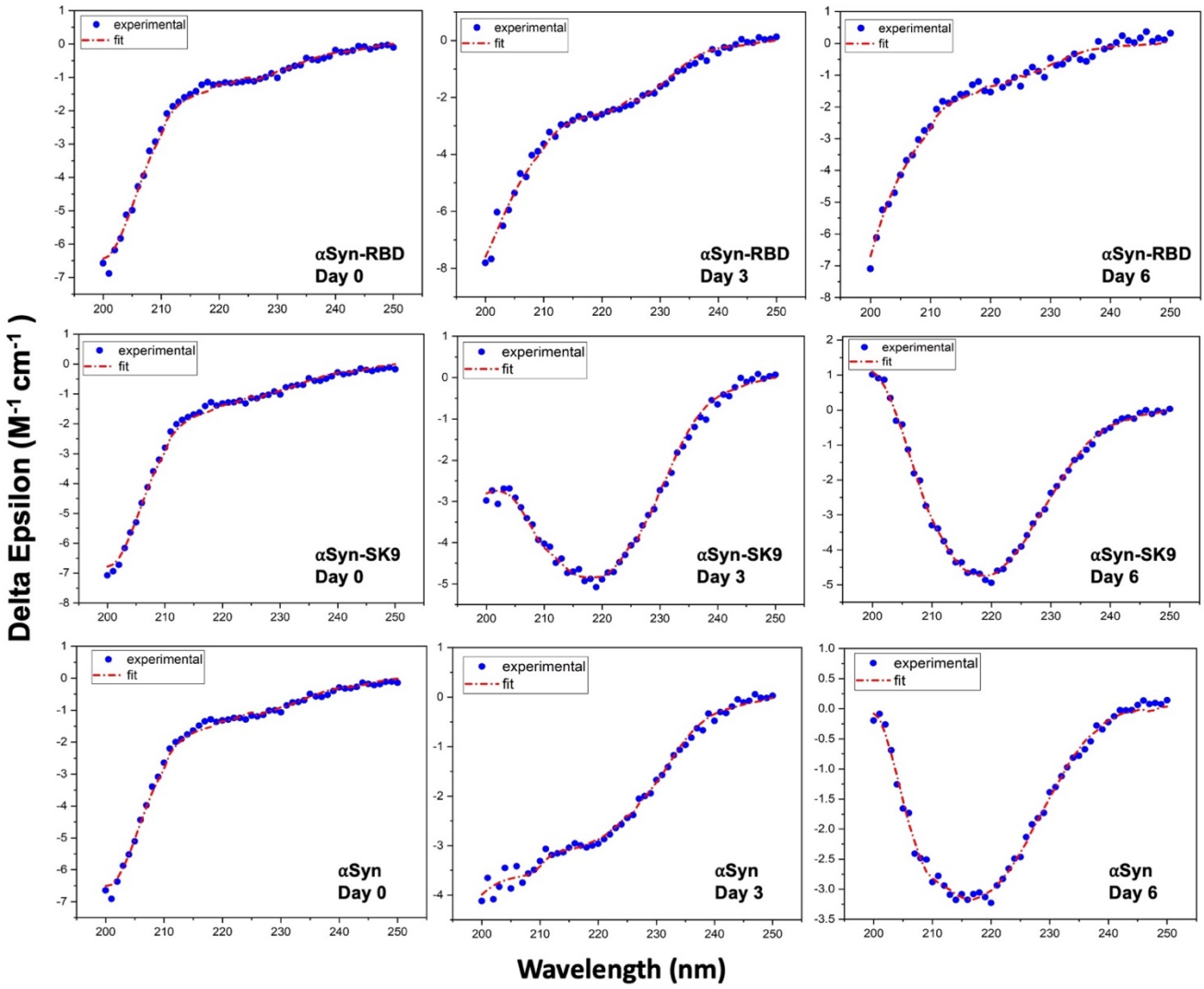

Figure S2. The fitted CD spectra of all αSyn systems for selected incubation time. The CD spectra (blue dots) of αSyn-RBD (top row), αSyn-SK9 (middle row), and αSyn control (bottom row) were fitted against the BeStSel algorithm (red dashed line). The spectra for fitting were selected from different incubation periods: day 0 (left column), day 3 (middle column), and day 6 (right column).

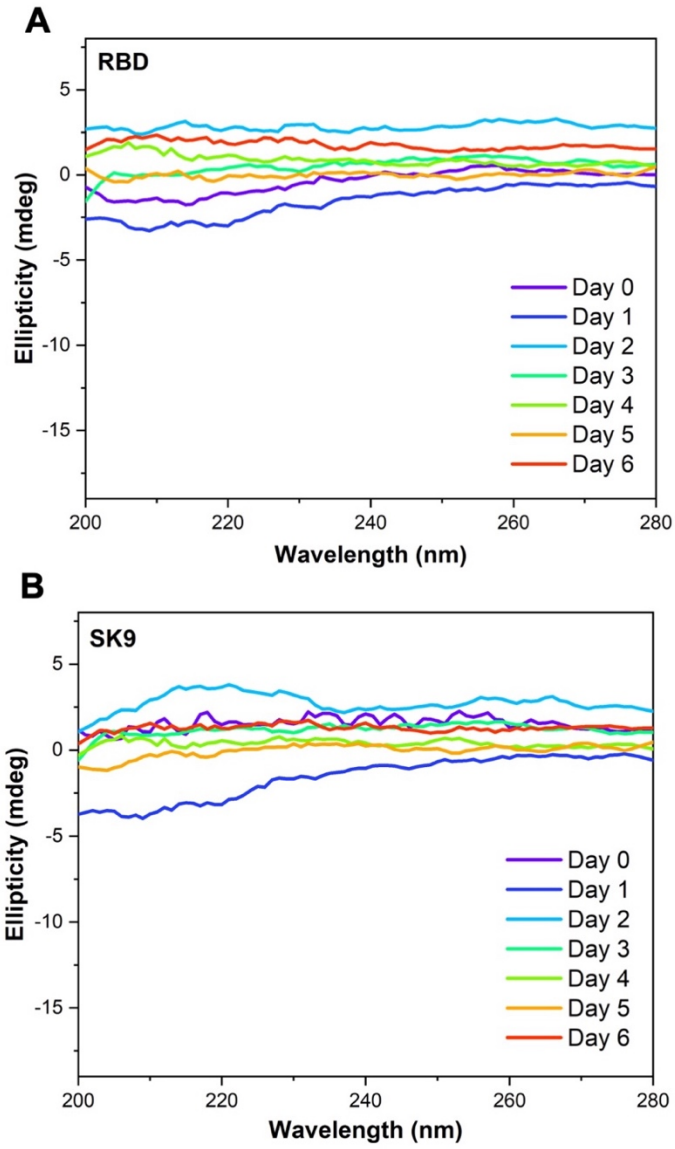

Figure S3. The control CD spectra of SARS-CoV-2 protein segments. A.) The CD spectra of 0.1 μM RBD from day 0 to day 6 measured on a daily interval. B.) The CD spectra of 5 μM SK9 from day 0 to day 6 measured on a daily interval. Each spectrum is an average of 10 scans.

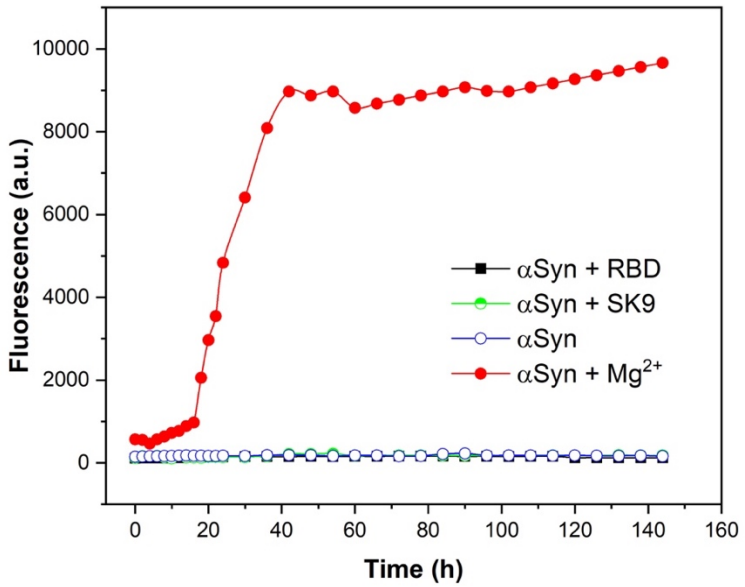

Figure S4. The Thioflavin T aggregation assay of αSyn-RBD, αSyn-SK9, and αSyn for six (6) days with two-hour increment for the first 24 h and six-hour increment until day 6. Each sample was excited at 446 nm and measured at 495 nm. An additional αSyn sample with Mg^{2+} ions was also analyzed as a positive control for amyloid fibrils.

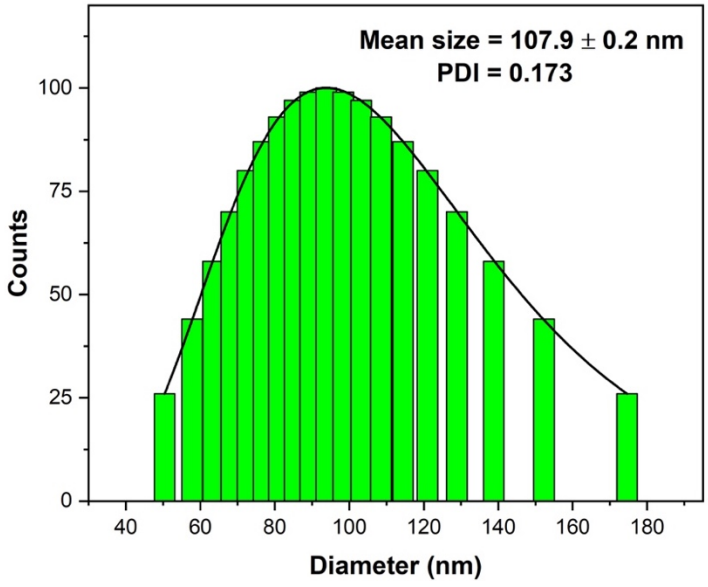

Figure S5. The particle size distribution of the small unilamellar vesicles (SUV) measured by dynamic light scattering. The plot of intensity counts against the hydrodynamic diameter (green bars) were fitted to the lognormal distribution (black line). Shown are the mean size and the polydispersity index (PDI) of the SUV.

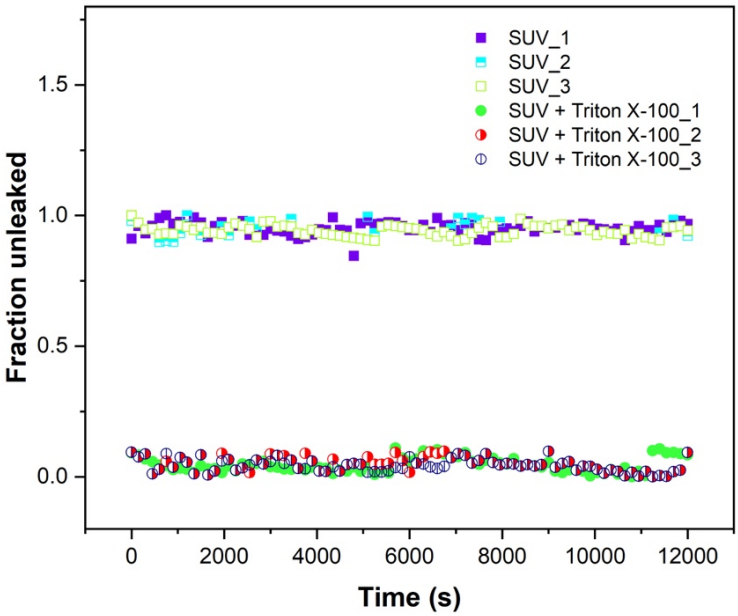

Figure S6. The leakage profiles of SUV alone and the SUV with Triton X-100 in three measurements. The SUV samples were added with PBS instead of αSyn solutions while the other SUV samples were treated with 0.1% Triton X-100. Both samples have DPX quencher.

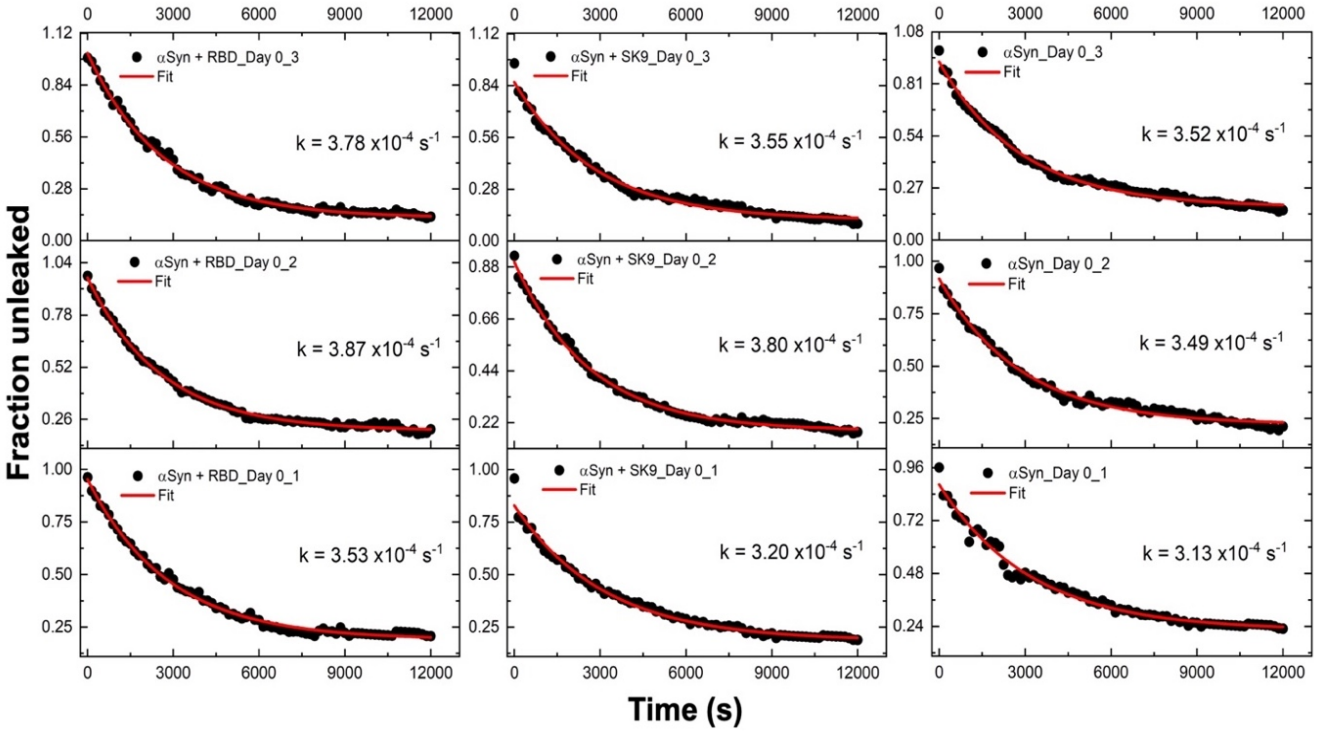

Figure S7. The individual fitting of the leakage experiments upon the exposure of the SUVs to αSyn-RBD (left column), αSyn-SK9 (middle column), and αSyn (right column) without prior incubation (day 0). The plot of fraction unleaked against time was fitted by single exponential decay using Levenberg-Marquardt algorithm in OriginPro 2018.

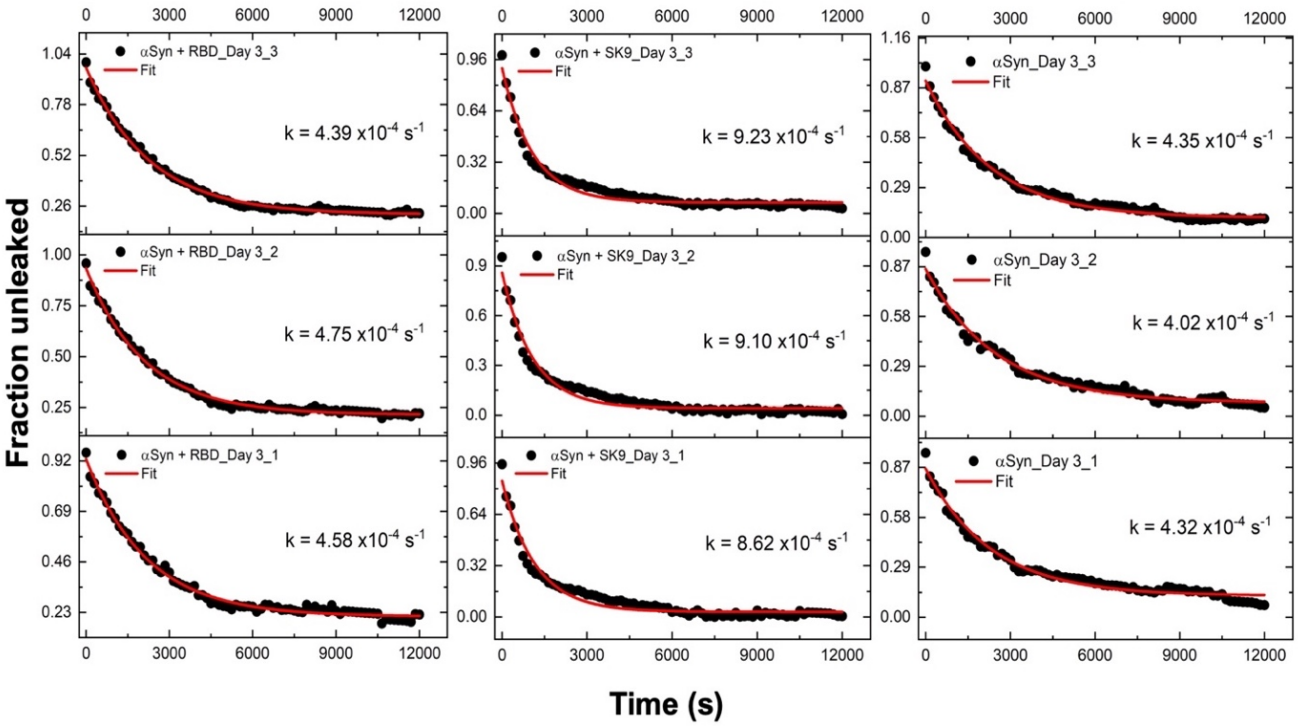

Figure S8. The individual fitting of the leakage experiments upon the exposure of the SUVs to αSyn-RBD (left column), αSyn-SK9 (middle column), and αSyn (right column), incubated for 3 days. The plot of fraction unleaked against time was fitted by single exponential decay using Levenberg-Marquardt algorithm in OriginPro 2018.

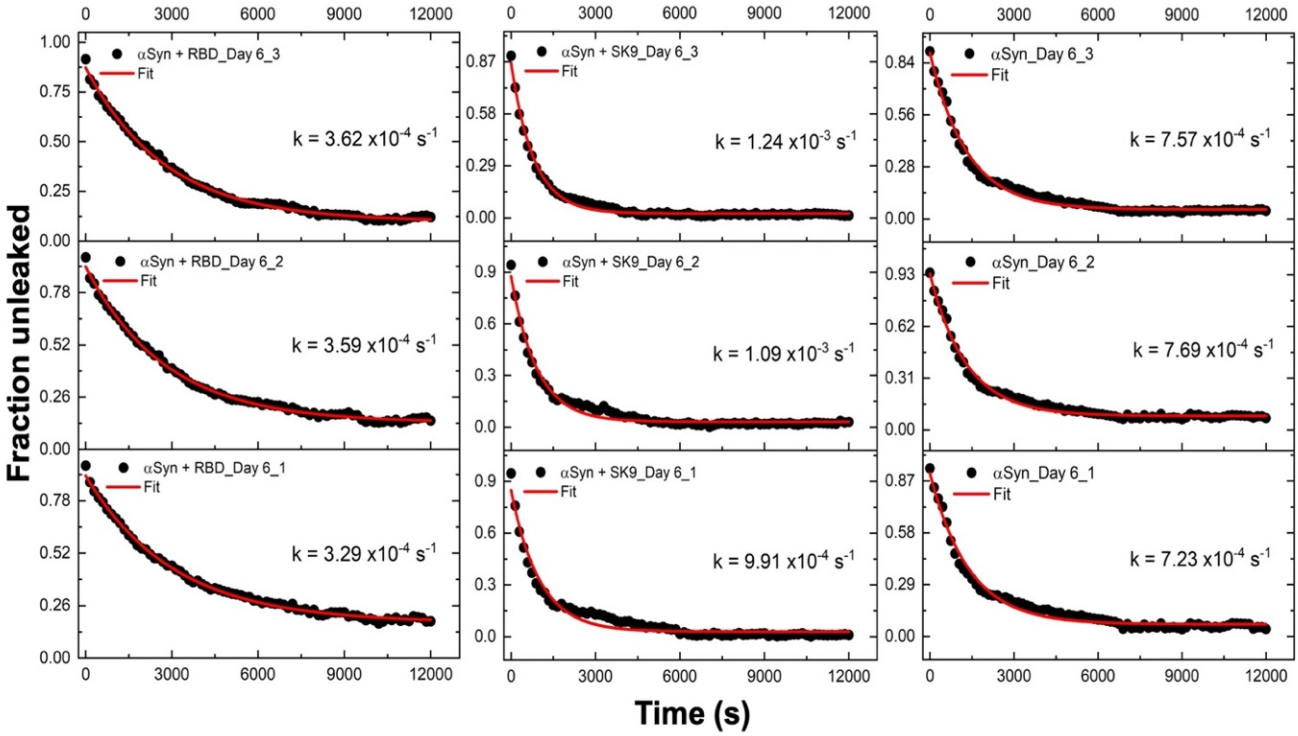

Figure S9. The individual fitting of the leakage experiments upon the exposure of the SUVs to αSyn-RBD (left column), αSyn-SK9 (middle column), and αSyn (right column), incubated for 6 days. The plot of fraction unleaked against time was fitted by single exponential decay using Levenberg-Marquardt algorithm in OriginPro 2018.

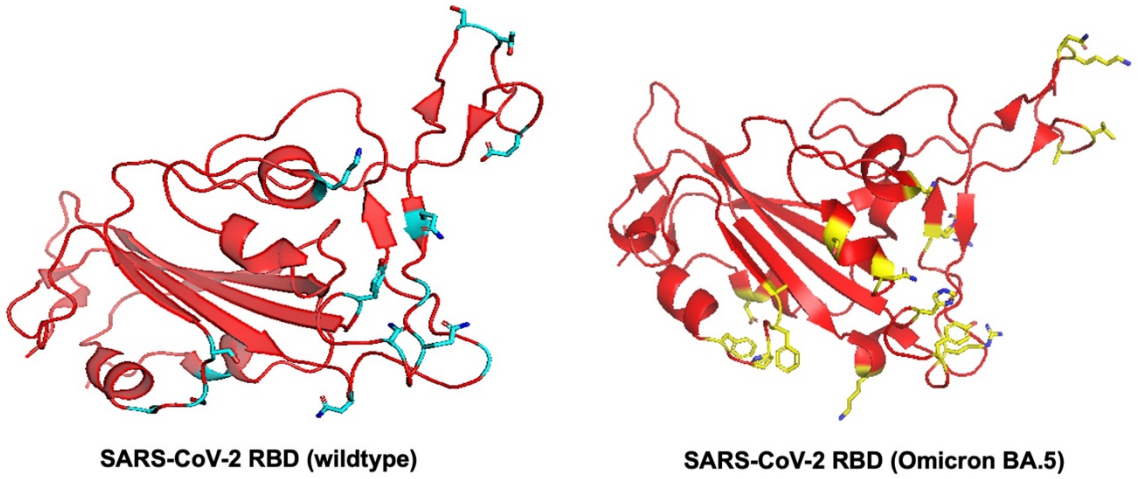

Figure S10. Comparison between the RBD of the wildtype (left) and that of the BA.5 Omicron variant (right). The involved residues of the wildtype RBD (blue) are shown prior to their mutations as reflected in the Omicron RBD (yellow). Detailed mutations are shown as follows: G339D, S371F, S373P, S375F, T376A, D405N, R408S, K417N, N440K, L452R, S477N, T478K, E484A, F486V, Q498R, N501Y, Y505H.[12]

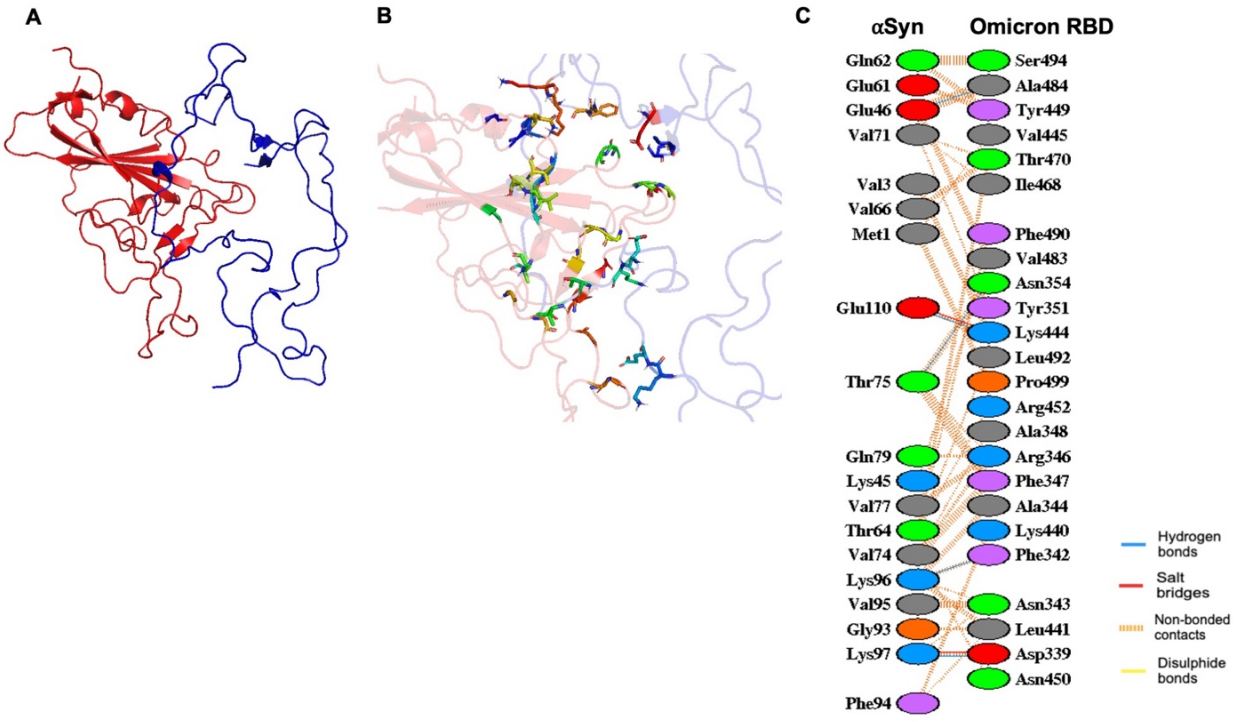

Figure S11. Molecular insights on the αSyn interaction with the Omicron (BA.5) RBD A.) The αSyn-RBD (Omicron) model obtained from HADDOCK 2.4 B.) The representation of αSyn-RBD (Omicron) binding interface C.) The detailed αSyn-RBD (Omicron) binding interface obtained from PDBsum. The αSyn-Omicron RBD interface involves two (2) salt bridges, five (5) hydrogen bonds, and one-hundred twelve (112) non-bonded contacts.

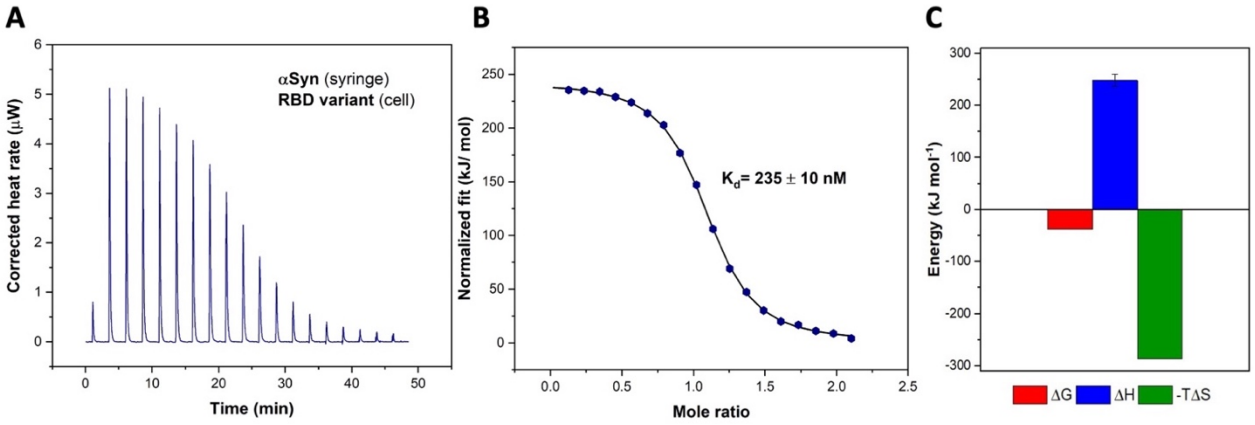

Figure S12. Isothermal titration calorimetry between alpha synuclein and the mutated variants. A.) Thermogram of alpha synuclein and Omicron RBD titration with the B.) Binding curve showing the binding affinity (K_d= 235 $\pm$ 10 nM), and C.) the thermodynamics of αSyn-RBD titration with ΔG (red), ΔH (blue), and -TΔS (green).

Table S1. The quantification of secondary structures the circular dichroism spectra of the αSyn systems at different incubation periods. Each spectrum was fitted using the BeStSel algorithm and the best fit was identified after a number of successive iterations.

System	Incubation period [a]	Secondary structure [b]				
		Random coil	Turn	Alpha helix	Anti-parallel beta sheet	Parallel beta sheet
αSyn-RBD	0	58.1	18.1	1.7	22.1	0
	3	49	13.5	9	28.1	0.4
	6	46.65	19.58	0	33.77	0
αSyn-SK9	0	58.9	16.5	1.3	23.3	0
	3	43.5	7	8.2	19.1	22.2
	6	42.76	5.79	6.39	15.18	29.87
αSyn	0	59.5	16.4	1.9	22.2	0
	3	46.15	12.59	13.19	18.58	9.49
	6	38	13.8	12.1	18.2	17.9

[a] Days of incubation. [b] Percentage secondary structure.

Table S2. The parameters derived from the fitting of the leakage profiles of αSyn-RBD, αSyn-SK9, and αSyn against the single exponential decay model. The time constant t_1 is the parameter from which the rate constant (k) is obtained, while y_0 is the offset and A_1 describes the amplitude of the decay. The parameters reduced-chi square (χ^2) and coefficient of determination (R^2) indicate the degree of fitness between the model and experimental data.

System	Incubation period [a]	Replicates	Single exponential decay model [b]				
			y_0	A_1	t_1 (1/k)	χ^2	R^2
αSyn-RBD	0	Trial 1	0.19084	0.76145	2829.291	0.000201	0.995
		Trial 2	0.20295	0.76231	2587.573	0.000119	0.997
		Trial 3	0.12303	0.88954	2647.308	0.000245	0.996
	3	Trial 1	0.21103	0.71683	2181.727	0.000294	0.991
		Trial 2	0.21497	0.71836	2107.105	0.000165	0.995
		Trial 3	0.21717	0.75267	2276.631	0.000132	0.996
	6	Trial 1	0.17529	0.72928	3041.605	0.000131	0.997
		Trial 2	0.13291	0.77522	2783.111	0.000141	0.997
		Trial 3	0.09922	0.77342	2764.297	0.000136	0.997
αSyn-SK9	0	Trial 1	0.18543	0.64375	3126.375	0.000345	0.988
		Trial 2	0.18611	0.71567	2630.446	0.000129	0.996
		Trial 3	0.11388	0.7453	2814.828	0.000409	0.990
	3	Trial 1	0.0319	0.81579	1160.276	0.00112	0.964
		Trial 2	0.04122	0.81759	1099.503	0.000929	0.969
		Trial 3	0.06872	0.83754	1083.032	0.000876	0.972
	6	Trial 1	0.02928	0.81899	1009.117	0.00106	0.963
		Trial 2	0.03039	0.84557	921.676	0.000561	0.983
		Trial 3	0.02352	0.84015	809.250	0.000195	0.992
αSyn	0	Trial 1	0.22181	0.66168	3198.246	0.000434	0.986
		Trial 2	0.22107	0.69476	2863.080	0.000353	0.990
		Trial 3	0.17142	0.75249	2838.250	0.000280	0.993
	3	Trial 1	0.12469	0.73885	2310.067	0.000693	0.981
		Trial 2	0.07806	0.77902	2490.374	0.000606	0.985
		Trial 3	0.11452	0.79642	2298.146	0.000468	0.989
	6	Trial 1	0.06843	0.84547	1382.797	0.000635	0.983
		Trial 2	0.08465	0.85044	1301.303	0.000350	0.990
		Trial 3	0.05119	0.84249	1320.687	0.000347	0.990

[a] Days of incubation. [b] $y = A_1 * \exp(-x/t_1) + y_0$

References

(1) Dai, X.; Fu, W.; Chi, H.; Mesias, V. S. D.; Zhu, H.; Leung, C. W.; Liu, W.; Huang, J. Optical Tweezers-Controlled Hotspot for Sensitive and Reproducible Surface-Enhanced Raman Spectroscopy Characterization of Native Protein Structures. *Nat. Commun.* **2021**, *12* (1), 1-9

(2) Tang, X.; Zhang, L.; Ma, T.; Wang, M.; Li, B.; Jiang, L.; Yan, Y.; Guo, Y. Molecular Mechanisms That Regulate Export of the Planar Cell-Polarity Protein Frizzled-6 out of the Endoplasmic Reticulum. *J. Biol. Chem.* **2020**, *295* (27), 8972–8987.

(3) Cheng, H. T.; Megha; London, E. Preparation and Properties of Asymmetric Vesicles That Mimic Cell Membranes. Effect upon Lipid Raft Formation and Transmembrane Helix Orientation. *J. Biol. Chem.* **2009**, *284* (10), 6079–6092.

(4) Micsonai, A.; Wien, F.; Kernya, L.; Lee, Y. H.; Goto, Y.; Réfrégiers, M.; Kardos, J. Accurate Secondary Structure Prediction and Fold Recognition for Circular Dichroism Spectroscopy. *Proc. Natl. Acad. Sci. U. S. A.* **2015**, *112* (24), E3095–E3103.

(5) Micsonai, A.; Wien, F.; Bulyáki, É.; Kun, J.; Moussong, É.; Lee, Y. H.; Goto, Y.; Réfrégiers, M.; Kardos, J. BeStSel: A Web Server for Accurate Protein Secondary Structure Prediction and Fold Recognition from the Circular Dichroism Spectra. *Nucleic Acids Res.* **2018**, *46* (W1), W315–W322.

(6) Jana, A. K.; Lander, C. W.; Chesney, A. D.; Hansmann, U. H. E. Effect of an Amyloidogenic SARS-COV-2 Protein Fragment on α-Synuclein Monomers and Fibrils. *J. Phys. Chem. B.* **2022**, *126* (20), 3648–3658.

(7) Honorato, R. V.; Koukos, P. I.; Jiménez-García, B.; Tsaregorodtsev, A.; Verlato, M.; Giachetti, A.; Rosato, A.; Bonvin, A. M. J. J. Structural Biology in the Clouds: The WeNMR-EOSC Ecosystem. *Front. Mol. Biosci.* **2021**, *8*, 1–7.

(8) Van Zundert, G. C. P.; Rodrigues, J. P. G. L. M.; Trellet, M.; Schmitz, C.; Kastritis, P. L.; Karaca, E.; Melquiond, A. S. J.; Van Dijk, M.; De Vries, S. J.; Bonvin, A. M. J. J. The HADDOCK2.2 Web Server: User-Friendly Integrative Modeling of Biomolecular Complexes. *J. Mol. Biol.* **2016**, *428* (4), 720–725.

(9) Xue, L. C.; Rodrigues, J. P.; Kastritis, P. L.; Bonvin, A. M.; Vangone, A. PRODIGY: A Web Server for Predicting the Binding Affinity of Protein-Protein Complexes. *Bioinformatics* **2016**, *32* (23), 3676–3678.

(10) Vangone, A.; Bonvin, A. M. J. J. Contacts-Based Prediction of Binding Affinity in Protein–Protein Complexes. *Elife* **2015**, *4*, 1–15.

(11) Laskowski, R. A. PDBsum New Things. *Nucleic Acids Res.* **2009**, *37*, 355–359.

(12) Tuekprakhon, A.; Nutalai, R.; Dijokaite-Guraliuc, A.; Zhou, D.; Ginn, H. M.; Selvaraj, M.; Liu, C.; Mentzer, A. J.; Supasa, P.; Duyvesteyn, H. M. E.; Das, R.; Skelly, D.; Ritter, T. G.; Amini, A.; Bibi, S.; Adele, S.; Johnson, S. A.; Constantinides, B.; Webster, H.; Temperton, N.; Klenerman, P.; Barnes, E.; Dunachie, S. J.; Crook, D.; Pollard, A. J.; Lambe, T.; Goulder, P.; Paterson, N. G.; Williams, M. A.; Hall, D. R.; Conlon, C.; Deeks, A.; Frater, J.; Frending, L.; Gardiner, S.; Jämsén, A.; Jeffery, K.; Malone, T.; Phillips, E.; Rothwell, L.; Stafford, L.; Fry, E. E.; Huo, J.; Mongkolsapaya, J.; Ren, J.; Stuart, D. I.; Screaton, G. R. Antibody Escape of SARS-CoV-2 Omicron BA.4 and BA.5 from Vaccine and BA.1 Serum. *Cell* **2022**, *185* (14), 2422–2433.